

Spiral instabilities: Mode saturation and decay

J. A. Sellwood^{1*} and R. G. Carlberg^{2†}

¹*Steward Observatory, University of Arizona, 933 N Cherry Ave, Tucson AZ 85722, USA*

²*Department of Astronomy and Astrophysics, University of Toronto, ON M5S 3H4, Canada*

4 October 2022

ABSTRACT

This paper continues a series reporting different aspects of the behaviour of disc galaxy simulations that support spiral instabilities. The focus in this paper is to demonstrate how linear spiral instabilities saturate and decay, and how the properties of the disc affect the limiting amplitude of the spirals. Once again, we employ idealized models that each possess a single instability that we follow until it has run its course. Remarkably, we find a tight correlation between the growth rate of the mode and its limiting amplitude, albeit from only six simulations. We show that non-linear orbit deflections near corotation cause the mode to saturate, and that the more time available in a slowly-growing mode creates the critical deflections at lower amplitude. We also find that scattering at the inner Lindblad resonance is insignificant until after the mode has saturated. Our objective in this series of papers, which we believe we have now achieved, has been to develop a convincing and well-documented account of the physical behaviour of the spiral patterns that have been observed in simulations by others, and by ourselves, for many decades. Understanding the simulations is an important step towards the greater objective, which is to find observational evidence from galaxies that could confront the identified mechanism.

Key words: galaxies: spiral — galaxies: evolution — galaxies: structure — galaxies: kinematics and dynamics

1 INTRODUCTION

Spiral instabilities have been reported in N -body simulations of rotating disc galaxy models for over 50 years (Miller, Prendergast & Quirk 1970; Hohl 1971; Hockney & Brownrigg 1974). This behaviour has revealed that spirals are fundamentally a collective phenomenon of many-body gravitational dynamics, but a satisfactory explanation for them has taken many years to emerge. We have developed, in a series of papers, an understanding of various dynamical processes that together furnish a compelling account for the behaviour in collisionless simulations, which would have been far more difficult to unravel had they included a gas component. These papers present a detailed analysis of simplified models that each build parts of the case. Not only does this piecemeal approach make it more difficult to see the whole picture, but the papers contain much technical detail that requires careful study. We therefore give below an overview in simple terms of the ideas we have developed. It is to be hoped that the same mechanism also accounts for the origin of self-excited spiral patterns in galaxies, but supporting observational evidence for this, or any other suggested excitation mechanism for spirals in galaxies, remains flimsy. See Sellwood & Masters (2022) for a full review of both the observed properties of spirals in galaxies and theoretical ideas to account for them.

Our fundamentally straightforward idea for the origin of spirals in simulations is as follows. A disc of particles having a moderate level of random motion is destabilized by non-smooth features in the distribution of angular momentum, which are inevitably present in all particle discs. A “groove,” or deficiency of particles over a narrow range of angular momentum, gives rise to one, or more, linearly unstable spiral modes that grow vigorously until saturating at $\lesssim 30\%$ relative overdensity before beginning to decay. The later stages of growth, saturation, and early decay enable a steadily rotating spiral pattern to be detectable for no more than ~ 10 rotations. As each spiral mode decays, it interacts with particles that are in resonance with the spiral, changing their angular momenta. This localized resonant scattering creates new grooves in the particle distribution that were not present before. The new grooves in turn give rise to fresh instabilities having differing pattern speeds, and perhaps rotational symmetries, that become new spiral patterns. The initial groove to seed this recurrent cycle in a real galaxy could be caused by resonance scattering as, say, an orbiting mass clump settles into the disk or by the near passage of a small companion or, in the unlikely circumstance that neither of these events happen, spiral disturbances could bootstrap out of the noise (Sellwood 2012).

In general, a disc possesses several spiral modes at any one time, each having a different pattern speed, rotational symmetry, and peaking in amplitude at a different time. The superposition of multiple modes causes the net spiral appear-

* E-mail: sellwood@as.arizona.edu

† E-mail: raymond.carlberg@utoronto.ca

ance to evolve continuously, and the overall pattern changes unrecognizably within one orbit period.

Since the scattering of particles by spiral waves is irreversible, the level of random motion in a collisionless disc rises, making it less responsive over time and spiral activity fades. However, it was noted by Oort (1962), and others, that spirals in real galaxies are most prominent in discs that are forming stars from a moderate fraction of gas. Sellwood & Carlberg (1984) demonstrated that mimicking the dissipative effects of gas by adding fresh star particles on near circular orbits could allow spiral activity to persist “indefinitely” (see also Carlberg & Freedman 1985; Toomre 1990; Aumer *et al.* 2016 and simulations of galaxy formation, reviewed *e.g.* by Vogelsberger *et al.* 2020).

The picture sketched in the previous few paragraphs is buttressed by several detailed papers. Sellwood & Kahn (1991) developed the theory of instabilities provoked by narrow features in the angular momentum density, and presented highly simplified simulations to illustrate them. The existence of multiple coherent waves having radially constant pattern speeds, first hinted at by Sellwood (1989), was confirmed by Sellwood & Carlberg (2014) in both 2D and 3D simulations having a thousand times more particles. That paper also demonstrated that later instabilities were caused by changes to the distribution function, since the same disturbances grew afresh when existing non-axisymmetric features were erased. Sellwood & Carlberg (2019) provided clear illustrations that scattering at the Lindblad resonances of an instability created grooves to seed new instabilities. Sellwood & Carlberg (2021) presented an animation¹ of how two superposed steady waves can give the impression of a swing-amplified transient. The present paper furnishes a study of the mechanism that arrests the exponential growth of a spiral instability, illustrates its subsequent decay, and how this behaviour depends on the mode growth rate.

Other ideas have been proposed for the origin of spirals in galaxies, which we generally find unconvincing. Toomre (1990) and D’Onghia *et al.* (2013) argue that spirals are responses to mass clumps orbiting within the disc; however, their models support small-scale, multi-arm patterns that do not resemble the large-scale, predominantly two-arm spirals of real galaxies (*e.g.* Davis *et al.* 2012; Hart *et al.* 2016; Yu *et al.* 2018). Dobbs & Baba (2014) reviewed the idea that spirals result simply from swing-amplification (Toomre 1981); not only do proponents of this idea offer no candidate for what is being amplified, but the empirical evidence they present results from a misinterpretation of their simulations, as explained in §6 of Sellwood & Carlberg (2021). Bertin *et al.* (1989), in a theory that is not based on simulations, argue that “grand design” spirals result from slowly-growing bi-symmetric modes that persist for many tens of rotations in sub-maximal discs. However the quiescent “basic state” they invoke for the disc is at variance with the unrelaxed phase space in the local disc of the Milky Way that was recently reported by Sellwood *et al.* (2019) from an action-angle analysis of *Gaia* DR2 data (Gaia collaboration 2018). Furthermore, this theory disregards the more vigorous insta-

bilities having $m > 2$ that are expected in sub-maximal discs (Sellwood 2011). Bertin (2014) argues that N -body simulations employ “too few particles”² to “properly capture” the damping of spirals at Lindblad resonances, despite the repeated demonstration (*e.g.* Sellwood & Lin 1989; Sellwood 2012; Sellwood & Carlberg 2014, 2019) of scattering of particles at Lindblad resonances, which is how spiral waves are absorbed and is the cause of the very instabilities the proponents of the density-wave theory choose to disregard.

As stated above, the purpose of this paper is to demonstrate the mechanism that causes a spiral instability to saturate, and to study its decay. In order to show this clearly, we employ simulations of a simplified model for the disc that initially possesses just a single spiral instability and follow its evolution until its decay has seeded new instabilities. In separate experiments, we also study the saturation of other modes that grow at differing rates.

2 TECHNIQUE

We employ the same model as Sellwood & Binney (2002), which is an otherwise stable disc model to which an initial groove is inserted to provoke a spiral instability. The reason that a groove is destabilizing, which was first given by Sellwood & Kahn (1991), is as follows.

2.1 Mechanism for linear growth

If all the particles were to pursue circular orbits then a groove would be a narrow feature in the surface density. Infinitesimal, sinusoidal distortions to the groove edges would bring high density material into the groove at some azimuths and conversely widen the groove at other phases of the distortion, creating bulges that corotate with the material on both edges. If the bulge on the outer edge of the groove were to lie ahead of that on the inner edge, then the gravitational attraction between the two bulges would remove angular momentum from the outer bulge, causing particles to sink further towards the disc centre, while those in the inner bulge would gain and therefore rise outward. Thus this phase relation between the two bulges creates a mild instability, even without the supporting response of the surrounding disc. The instability is still present in a disc with random motion, as long as the angular momentum distribution of the particles has a deficiency over a narrow range. In this case, however, random motions blur the density variations and thereby reduce the growth rate.

The growing distortions on the groove edges cause sinusoidal changes to the surface density around the groove, which therefore provoke a supporting response from the surrounding disc (Julian & Toomre 1966). The vigour of the large-scale supporting response, which is directly related to swing-amplification (Goldreich & Lynden-Bell 1965; Julian & Toomre 1966; Toomre 1981; Sellwood & Masters 2022), varies with the disc properties, and generally strongly enhances the mild growth rate of the groove instability that would be expected in its absence (Sellwood & Kahn 1991).

¹ Reproduced as

http://www.physics.rutgers.edu/~sellwood/supp_material.html, and in the supplementary material of Sellwood & Masters (2022).

² *NB.*, Sellwood (2012) employed up to $N = 5 \times 10^8$

Table 1. Default numerical parameters

Grid points in (r, ϕ, z)	230×256
Grid scaling	$R_0 = 10$ grid units
Active sectoral harmonics	see text
Softening length	$R_0/20$
Number of massive particles	6×10^6
Number of test particles	6.8×10^3
Time-step	$0.08R_0/V_0$
Time step zones	5

2.2 Adopted model

Our disc model is a half-mass Mestel disc having an initial $Q = 1.5$, with the distribution function (DF) given by [Binney & Tremaine \(2008\)](#). In order to limit its radial extent, the disc is tapered by a central cutout (index $\nu = 4$) and outer taper (index $\mu = 6$, centered on $R = 15$), that are both gentle enough so as not to be destabilizing. The surface density of the remaining disc is close to its untapered value over the range $2 \lesssim R \lesssim 10$. This model was predicted by [Toomre \(1981\)](#), and confirmed in simulations by [Sellwood \(2012\)](#), to have no linear instabilities whatsoever.

In order to provoke a spiral instability, we add a groove to this doubly tapered disc, f_0 . The groove has a Lorentzian function form, so our final DF is

$$f(E, L) = f_0(E, L) \left[1 + \frac{\beta w_L^2}{(L - L_*)^2 + w_L^2} \right]. \quad (1)$$

The first simulation we present in this paper uses values for the groove parameters adopted in [Sellwood & Binney \(2002\)](#) namely: depth $\beta = -0.4$, width $w_L = 0.2$, and central $L_* = 6.5$. In §4 we report the effects of changing the Q of the Mestel disc and the parameters of the groove.

The tapers and groove remove mass from the disc, but we ensure that the central attraction is $a_R = -V_0^2/R$ at all radii, implying a rigid halo and preserving the disc equilibrium. [Sellwood \(2021\)](#) verified that spiral dynamics is very little affected when a live halo is substituted for a rigid one.

Here, and throughout the paper, we use units such that $G = V_0 = R_0 = 1$, where V_0 is the circular speed of the Mestel disc and R_0 is the central radius of the inner cut out. Our unit of time is therefore $\tau_{\text{dyn}} = R_0/V_0$.

We select particles from this DF (eq. 1) using the method described in the appendix of [Debattista & Sellwood \(2000\)](#), and place copies of each particle regularly around a circle to create a quiet start ([Sellwood 1983](#)).

2.3 GALAXY code

The particles in our simulations move over a 2D polar mesh. The gravitational attractions between the particles are calculated at grid points and interpolated to the position of each particle. A full description of our numerical procedures is given in the on-line manual ([Sellwood 2014](#)) and the source code is available for download. Table 1 gives the values of the numerical parameters adopted for most simulations presented in this paper, which indicates that we typically employ ten times more particles than did [Sellwood & Binney \(2002\)](#). We note where these values were changed.

As usual, we measure non-axisymmetric distortions of the distribution of the N massive particles using an expansion in

logarithmic spirals:

$$A(m, \gamma, t) = \frac{1}{N} \sum_{j=1}^N \exp[im(\phi_j + \tan \gamma \ln R_j)], \quad (2)$$

where (R_j, ϕ_j) are the polar coordinates of the j th particle at time t , m is the sectoral harmonic, and γ is the (radially constant) angle of the spiral component to the radius vector, which is the complement to the pitch angle.

For this study, we also introduce a set of 34 rings, each having 200 equally spaced test particles, spanning the radial range of the principal mode $1.5 \leq R \leq 12.5$. These massless particles have initially circular orbits, but move in response to the central attraction and the disturbance forces from the massive disc particles. We find that their behaviour provides valuable additional information about the response of the disc to the growing mode.

3 RESULTS

3.1 Imposed bisymmetry

As reported by [Sellwood & Binney \(2002\)](#), the model described in §2.2 with disturbance forces confined to $m = 2$, possessed a single strong instability. Note we employed $N = 60$ million particles for this first simulation. Figure 1 presents the amplitude evolution of six of the $m = 2$ logarithmic spiral coefficients (eq. 2) over the second half of the evolution; the first half is dominated by exponential growth from low amplitude. The lines for different values of $\tan \gamma$ are parallel to $t \simeq 280$, indicating the disturbance has a fixed shape while growing exponentially, as expected for a normal mode. The trailing spiral terms $\tan \gamma = 2$ and 3 have the largest amplitude while the leading $\tan \gamma = -1$ is the smallest shown, and this leading/trailing bias arises because the disc response to the growing bisymmetric distortion around the groove ([Sellwood & Kahn 1991](#)) is closely related to swing-amplification, as explained in §2.1 above. Clearly, the instability saturates around $t \sim 300$, after which the shape of the disturbance changes.

The quiet start enabled us to fit a mode ([Sellwood & Athanassoula 1986](#)) to the simulation data over the whole growing phase. The best fit eigenfrequency of the mode is $\omega = m\Omega_p + i\beta = 0.282 \pm 0.000 + (0.046 \pm 0.001)i$, with the uncertainties indicating the full range of values from different time intervals and choices of fitted coefficients. Fits over time ranges to $t = 280$ are excellent and leave tiny residuals after subtracting this single mode from the data. This measured frequency is the same as that reported by [Sellwood & Binney \(2002\)](#), but the larger number of particles employed here gives the mode a lower seed amplitude and the time of mode saturation is therefore about 30 dynamical times later.

The radii of the principal resonances for circular orbits of an m -armed spiral lie where

$$m(\Omega_p - \Omega) = l\kappa, \quad (3)$$

with $\Omega \equiv V_0/R$ being the angular frequency of a circular orbit, $\kappa = \sqrt{2}V_0/R$ the epicyclic frequency in the Mestel disc, and $l = 0, \pm 1$. The corotation resonance has $l = 0$, $l = -1$ for the inner, and $l = +1$ for the outer, Lindblad resonance. The Lindblad resonances approximately limit the radial extent of

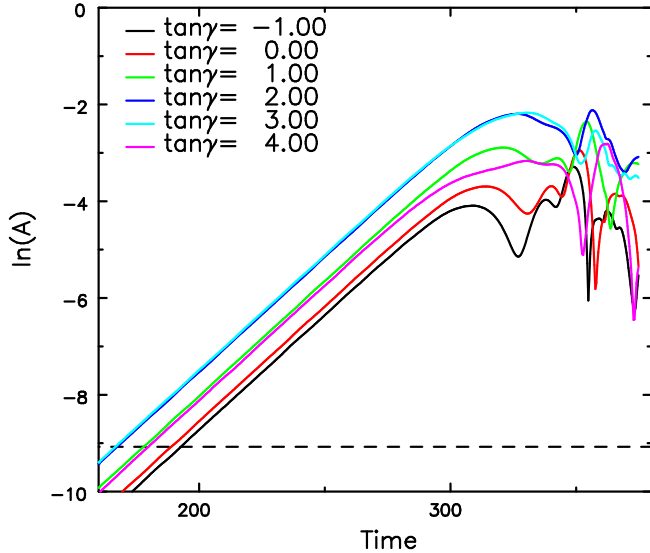


Figure 1. The second half of the amplitude evolution of several components of the logarithmic spiral transforms (eq. 2). The horizontal dashed line marks the amplitude expected if the particles were randomly distributed. The quiet start ensures that the initial amplitude is much lower at first, and each coefficient grows exponentially until the instability saturates at $t \sim 300$.

spiral modes. For an $m = 2$ disturbance having $\Omega_p = 0.141$ (this case), $R_{CR} = 7.09$, $R_{ILR} = 2.08$, and $R_{OLR} = 12.1$.

3.2 Orbit deflections

Figure 2 shows the evolution of rings of test particles that spanned the radial range of the linear instability. The red circle marks the radius of corotation at $R_{CR} = 7.09R_0$, while the cyan colored particles are those in the two rings each closest to the Lindblad resonances. Each panel is rotated through an angle $-\Omega_p t$ in order that the orientation of the disturbance changes little from frame to frame. The sense of rotation of the disc is counter-clockwise. Particles that have crossed the corotation resonance (CR) since the start are colored green or blue, other particles have not crossed the CR.

Although the instability has been growing exponentially from the start, its amplitude at $t = 256$ is still low and has created barely noticeable distortions of the rings. Inside the CR, the orientation of the mild oval distortions shifts with radius, creating the spiral density concentrations. Notice that the rings near the Lindblad resonances, coloured cyan, remain only mildly oval until after $t = 300$. Larger distortions near corotation become apparent after $t = 280$ that differ for particles at differing phases relative to the growing and rotating disturbance. Some particles have moved inwards, and have begun to run ahead of their unperturbed motion. At the same time, we also see that other particles have risen outwards and begun to lag behind. This behaviour is accounted for as follows.

Any particle, whether massive or not, near to corotation moves slowly with respect to the spiral perturbation and therefore experiences almost steady forcing from the wave. Particles orbiting just behind a density excess are attracted forward by it and therefore gain angular momentum. However, the consequence of gaining significant angular momen-

tum from a large-amplitude disturbance is that the particle moves onto an orbit having a larger guiding centre radius, and its angular frequency about the galaxy centre therefore decreases. Conversely, particles just ahead of the perturbation are pulled back, lose angular momentum and sink inwards, where they orbit at higher frequency. These changes to the guiding centre radius may cause the particle to cross corotation, and therefore to reverse its sense of motion relative to the disturbance, as shown by the coloured particles in Figure 2. This is, of course, part of the explanation for the phenomenon of radial migration (Sellwood & Binney 2002). The distance from corotation within which the anomalous orbit reversals in the corotating frame occur, which for a steady perturbation is known as the Hill radius (Binney & Tremaine 2008), grows with the amplitude of the spiral potential and is negligible at small amplitude.

Note that the behaviour in Figure 2 is simplified because the unperturbed orbits were circular and disturbance forces arose from only a single sectoral harmonic. The net response of the massive particles that generally have non-circular orbits would be blurred by their random motion, but the guiding centres of those orbits would follow the pattern illustrated, at least for those having small initial epicycles.

3.3 Saturation mechanism

For a linearly unstable mode, the first-order orbit deflections due to the growing disturbance potential create a density response that gives rise to the perturbing potential, which is the necessary self-consistency condition for a mode. First order changes to orbits in the disc may be computed as mild departures from their unperturbed orbits (*e.g.* Kalnajs 1971; Binney & Tremaine 2008) for as long as the disturbance amplitude remains small. As the amplitude rises, however, the approximation that the perturbed orbits can be computed as small departures from their unperturbed orbits breaks down, because either the perturbations become too large for first order theory to be adequate, or changes to the unperturbed orbits can no longer be ignored, or both.

Two examples of changes to the unperturbed orbits are: (a) a bar forming mode saturates when the orbits become trapped by the bar potential as its amplitude rises, and (b) the amplitude reaches that at which orbit distortions become large. In either case, the self-consistency requirement of an exponentially growing mode breaks down and the instability saturates. This is borne out for the present case by the evidence in Figure 2; linear growth of the mode ends around time 300 (Figure 1), which is when the shapes of the orbits near the CR begin to depart from the simple elliptical distortions that would be predicted by linear perturbation theory. Orbit reversals in the rotating frame, which can be thought of as a slightly different form of trapping (Sellwood & Binney 2002), cause the density response to the growing potential to disperse, whereas prior to their onset the mild deflections reinforced the growing mode.

Figure 3 displays the relative overdensity of bisymmetric distortions of the surface density at times during the later stages of the simulation, and the radii of the principal resonances of the first mode are marked. The dashed curves, which peak somewhat inside corotation, show the amplitude still growing, although the growth rate is beginning to slow by $t = 296$. Note also that the linear mode amplitude drops

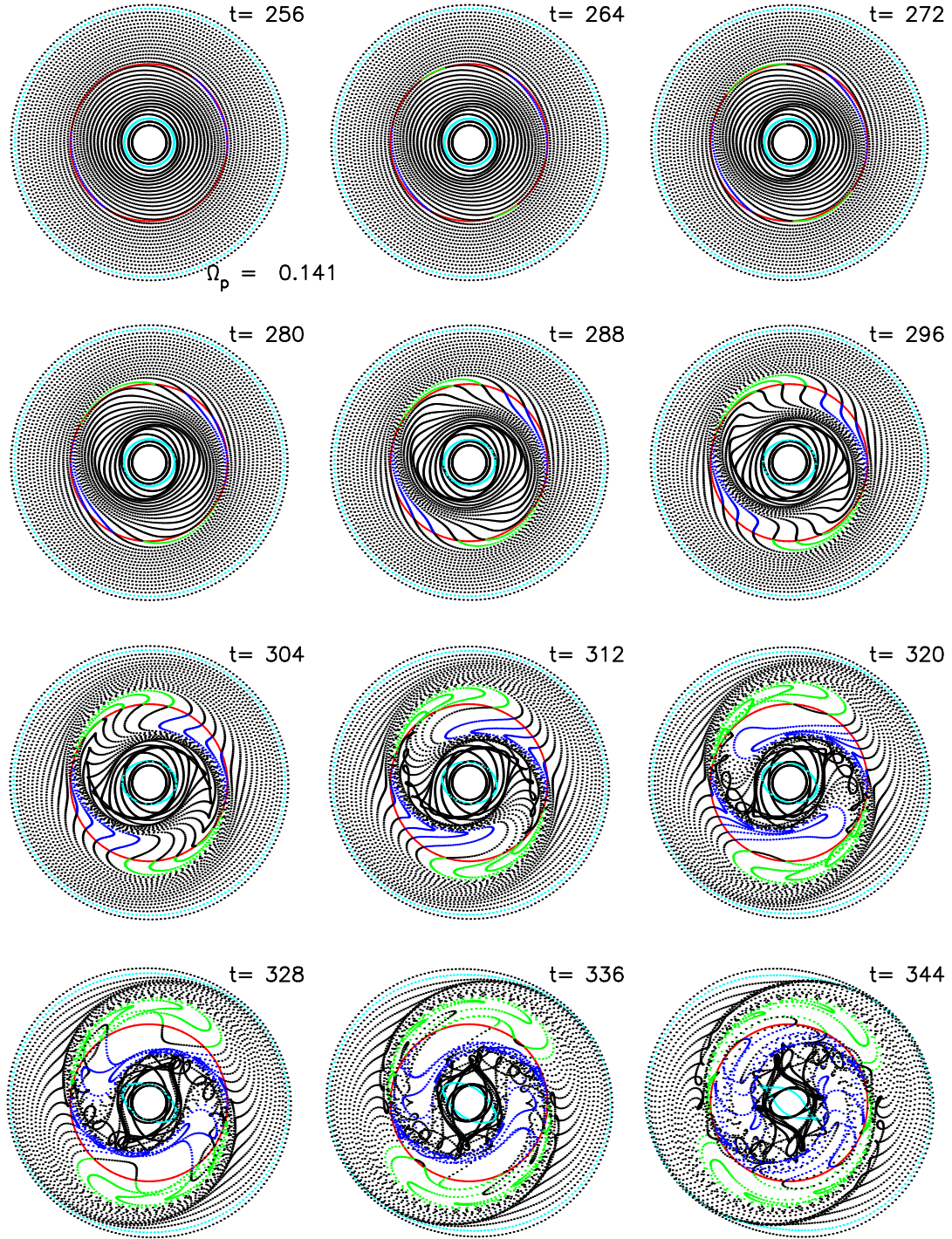


Figure 2. Snapshots showing the positions of the test particles, that had initially circular orbits, over a short time interval around the time that the spiral instability saturates. The red circle marks the corotation radius of the linear instability, which has the estimated pattern speed $\Omega_p = 0.141$, and the model rotates counter-clockwise. Each panel is rotated through an angle $-\Omega_p t$ in order that the orientation of the disturbance changes little from frame to frame. Green (outward movers) and blue (inward movers) particles have crossed the corotation resonance since the start, those that are black are the same side as at the start. The two rings highlighted in cyan are those closest to the Lindblad resonances, and remain only mildly distorted until well after the mode saturates.

precipitously towards the ILR. Thus for the groove mode, the important process that causes the instability to saturate is the change in the shapes of the orbits near to corotation, which happens over a short period (Figure 2).

Binney & Tremaine (2008, their §8.3.1) find that the Hill

radius for a steady perturbing potential varies as the cube root of the perturber mass, or amplitude and is therefore tiny as the mode starts to grow. In our case, the disturbance is growing exponentially, but the amplitude dependence they find may still account for the sudden change of

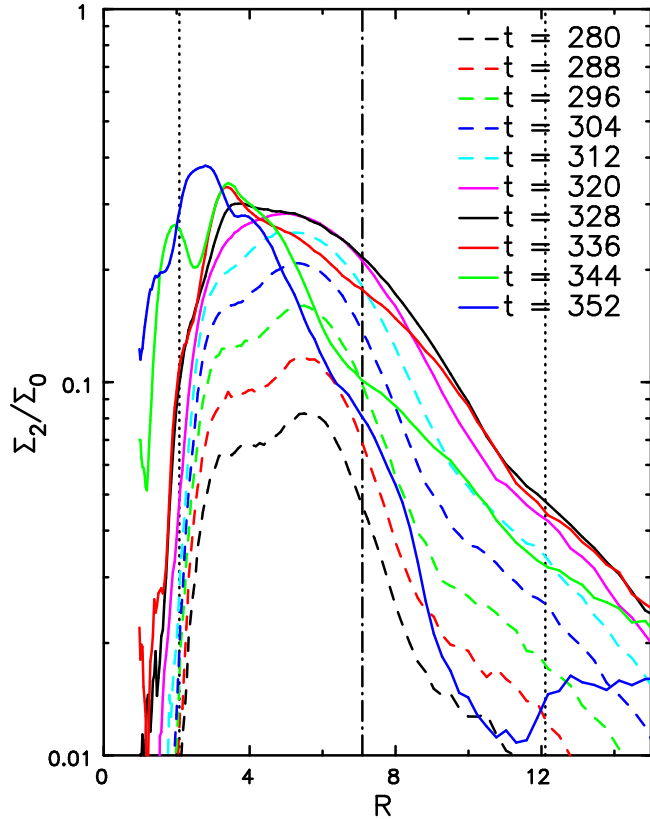


Figure 3. The time evolution of the relative overdensity of bisymmetric distortions of the surface density in the later stages of the simulation after the first mode has saturated. The dashed curves show the mode amplitude still growing, although the growth rate is beginning to slow by $t = 304$. The vertical dash-dot line marks the corotation radius, and the dotted lines the radii of the Lindblad resonances. The other curves are described in the text.

behaviour we illustrate for the test particles in Figure 2. The massive particles are similarly affected, as we show in §3.6, which causes the instability to saturate. This idea was outlined by Sellwood & Binney (2002) and restated by Sellwood & Carlberg (2014), but without supporting evidence, such as that shown in Figures 1, 2, & 3.

Notice the pronounced amplitude contrast between the spiral in the inner and outer disc in our Figure 3, which was also evident in the “dust-to-ashes” figure in Toomre (1981). In the absence of an external torque on the disc, the angular momentum content, or wave action, of the two parts of the wave must be equal, though of opposite sign. Sellwood & Masters (2022) argued that conservation of wave action in the shrinking geometric area as the wave propagates inwards keeps the amplitude of the spiral high, whereas conversely the spiral amplitude diminishes as it spreads outward beyond corotation.

3.4 Subsequent evolution

Figure 1 shows the growth rate eases at $t \sim 300$, but both there and in Figure 3 the disturbance density over much of the radial range continues to rise to $t \simeq 320$. Later, to $t = 352$ the wave amplitude continues to increase well interior to corotation, while decreasing toward and beyond the CR,

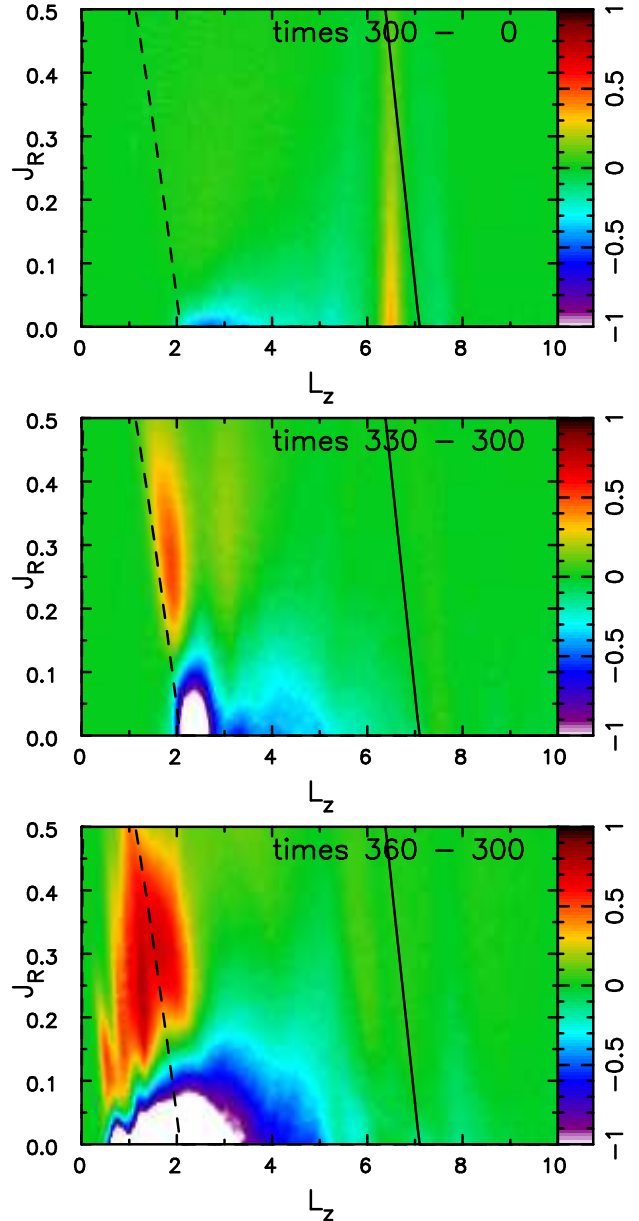


Figure 4. Changes to the relative density of particles in the space of angular momentum and radial action between times 0 and 300 (top), times 300 and 330 (middle) and times 300 and 360 (bottom). The solid line marks the locus of the corotation resonance of the first mode, the dashed line that of its ILR. Notice that although the first mode had begun to saturate by $t = 300$, strong scattering at the ILR did not occur until later. The most evident change in the top panel is simply that the initial groove, which was inside corotation has filled in.

providing some evidence that the disturbance is travelling away from the CR at late times.

Linear theory (Toomre 1969) predicts that a trailing spiral wave packet is carried away from corotation, both inward and outward, at the group velocity. It travels radially until it is absorbed at a Lindblad resonance (Lynden-Bell & Kalnajs 1972). The absorption of the first disturbance at its ILR is partly obscured in Figure 3 by the new vigorous instability that develops in the inner disc, which is probably the reason

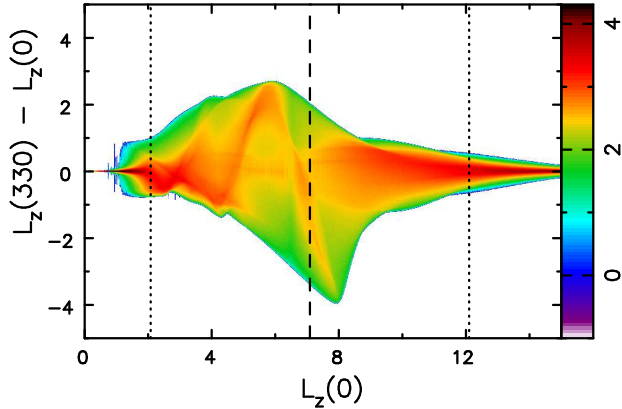


Figure 5. Changes to the angular momenta of the massive particles between times 0 and 330. Radial migration is again clear in this rerun of the case reported by [Sellwood & Binney \(2002\)](#), but here with 100 times more particles. The dashed line marks the angular momentum of circular orbits at corotation, the dotted lines the Lindblad resonances. The colour scale shows the logarithm of the number of particles in each pixel.

that the last two curves in this Figure show the disturbance density rising again near the ILR.

In fact, the spiral persists for some time and has not fully decayed even by $t \sim 352$, which is more than one full turn of the disturbance after saturation ($2\pi/\Omega_p = 43.6$ dynamical times). A second instability, also reported by [Sellwood & Binney \(2002\)](#), is growing at this time, and superposition of two or more waves causes the transforms of the entire disc, shown in Figure 1, to appear incoherent from then to the end of the simulation.

3.5 Resonant scattering

Scattering of particles at the Lindblad resonances is second order in the perturbation amplitude ([Lynden-Bell & Kalnajs 1972](#)), and therefore starts as the instability begins to grow from very low amplitude. But here we show that most scattering occurs after the mode has saturated. This is because the instability has acquired a store of angular momentum ([Lynden-Bell & Kalnajs 1972](#)) that is carried away from corotation at the group velocity ([Toomre 1969](#)).

The radii of the principal resonances for circular orbits were defined in eq. (3) and evaluated there for this mode. The angular momenta of more general non-circular orbits that are also in resonance decrease as the orbits become more eccentric.

Figure 4 shows changes to the density of particles in action space over the time interval from the start to when the mode saturates (top panel) and two short periods thereafter (middle and bottom panels). The contrast between the top and the other two panels makes it clear that most scattering at the ILR occurs while the mode decays, as the angular momentum stored in the disturbance drains onto the resonance. Note that the changes at the ILR in the middle panel are not perfectly aligned with the resonance line and there is an apparent weaker scattering feature at $L_z = 3$ and large J_R . Since we computed actions assuming an axisymmetric potential, both these discrepancies from expectations may be due to the continued presence of the spiral. In particular, they dis-

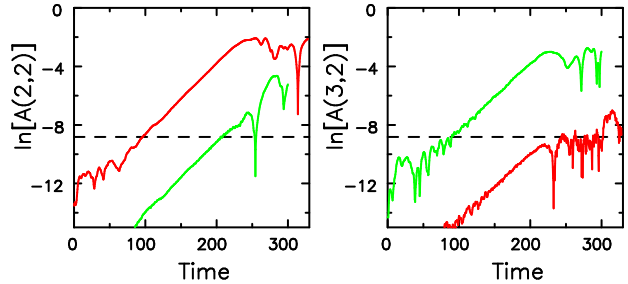


Figure 6. The amplitude evolution of a trailing $m = 2$ coefficient on the left and a trailing $m = 3$ coefficient on the right in two simulations. The red lines are from a case in which the $m = 2$ seed amplitude was enhanced while $m = 3$ seed amplitude was enhanced for the results reported by the green lines. In both cases, the disturbance forces included multiple sectoral harmonics, and the linear growth of modes having comparable growth rates can be seen in both panels.

appear by $t = 360$ when the spiral is weaker (bottom panel) although additional features at small L_z associated with the second mode have appeared by then.

While [Sellwood & Carlberg \(2019\)](#) convincingly demonstrated that scattering at a Lindblad resonance seeded a new instability, it is clear from this discussion that the new instability may already have begun to grow before the process of resonance scattering has completed.

3.6 Radial migration

It is remarkable that there is no strong feature in any of the panels of Figure 4 near corotation at $L_z = 7.09$, which should be where radial migration is strongest ([Sellwood & Binney 2002](#)). The top panel shows only that the initial groove, which is inside corotation for the mode, has filled, leaving faint deficiencies on either side. Notice that corotation for the mode is at a larger radius than the groove, even though [Sellwood & Kahn \(1991\)](#) predicted it should lie at the groove centre; this difference is due to curvature in the global model, which was neglected in their local analysis.

Figure 5 confirms that most massive particles close to corotation have in fact suffered large changes to L_z by $t = 330$, a time when the spiral is fading, but still visible. These changes were also illustrated by the behaviour of the test particles in Figure 2. The absence of a corresponding feature in Figure 4 reflects the fact that radial migration really does not heat the disc and the guiding centres of orbits are simply interchanged. Note that the changes at the Lindblad resonances in Figure 5 are much smaller than those at corotation.

3.7 Including other sectoral harmonics

While instabilities having different rotational symmetries are decoupled at small amplitude, that ceases to be true at large amplitude. As exemplified in Fig. 2, orbit deflections ceased to be sinusoidal even as the forcing terms, in this case, remained so. Therefore, disturbances at different m become coupled at large amplitude, and a full description of the non-linear behaviour requires including multiple sectoral harmonics, as we now describe.

A slight complication is that our adopted model possesses

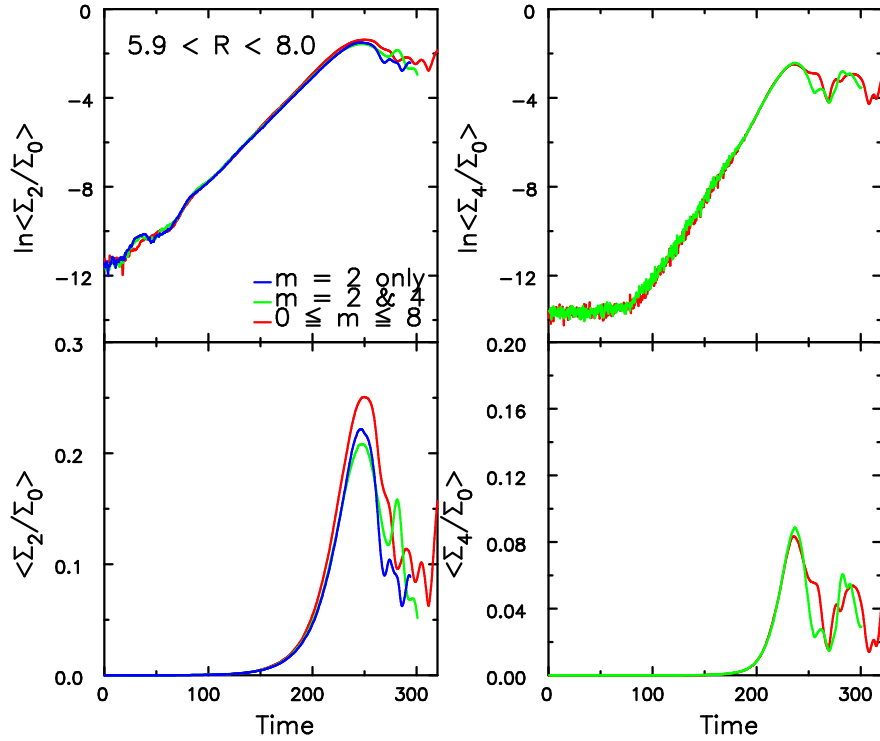


Figure 7. The amplitude evolution of the relative disturbance density, averaged over the given radial range that includes corotation of the $m = 2$ mode. The upper panels use a logarithmic scale for the amplitude, while the lower panels show the same data on a linear scale; the left panels report the $m = 2$ amplitude and the right panels the $m = 4$ amplitude from the same simulations. The time axis applies to the simulation shown by the red curve, while the other cases were shifted in time in order that they pass through the same point in the middle of the linear growth. Disturbance forces in the three simulations, in which the $m = 2$ seed amplitude was enhanced, were computed using the indicated numbers of sectoral harmonics in the left panels, and the same colours are used in the right hand panels, although there can obviously be no data in those panels from the $m = 2$ only case.

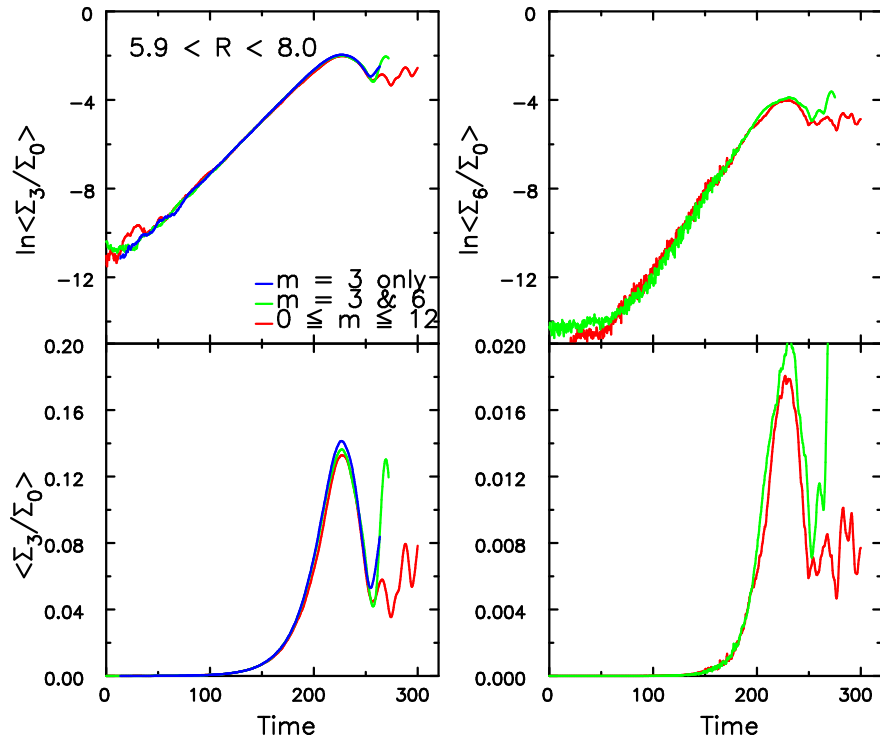


Figure 8. As for Figure 7 but from simulations that started with the $m = 3$ amplitude enhanced.

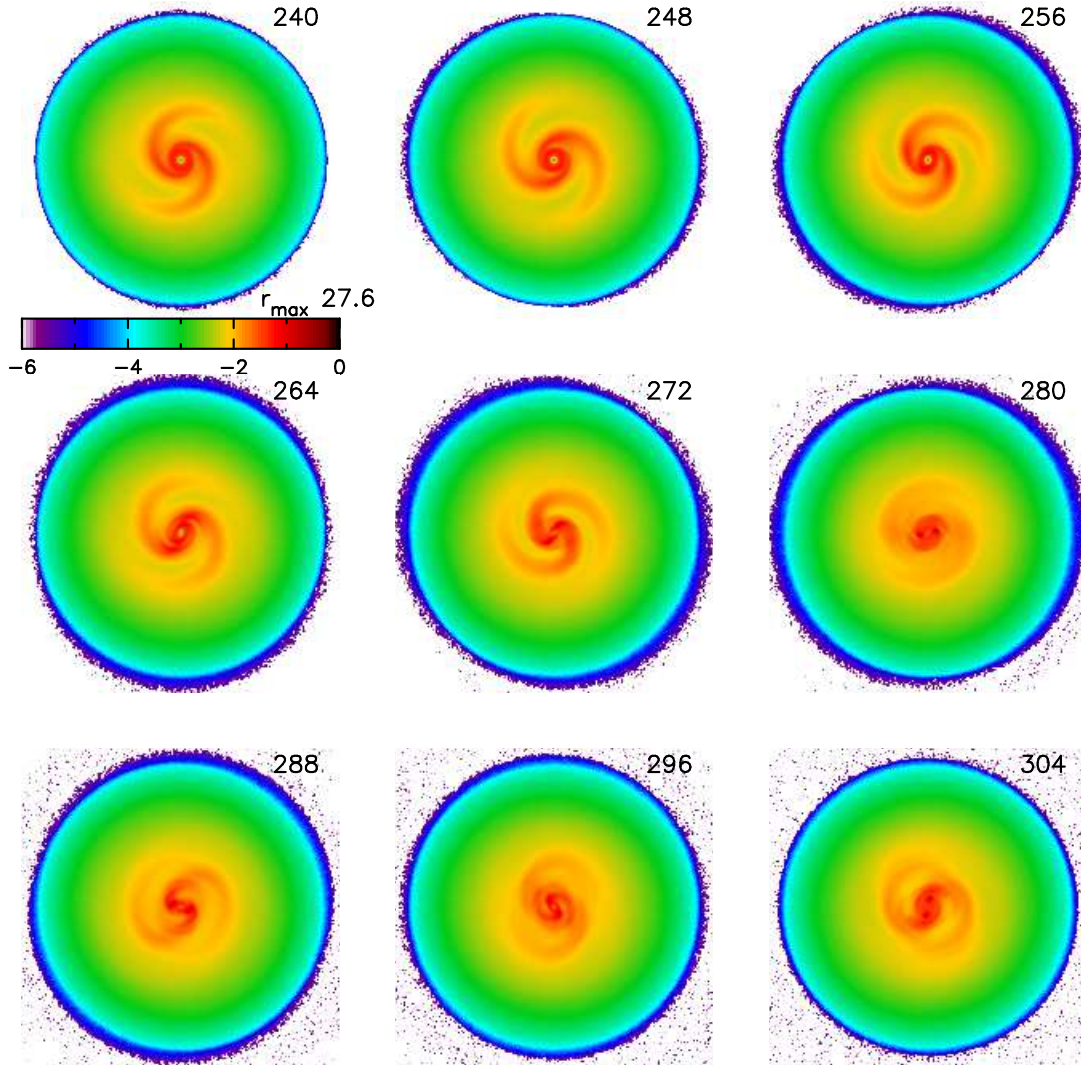


Figure 9. Snapshots showing the logarithm of the disc surface density over the time interval as the mode saturates ($t \sim 250$) and continuing to much later. Notice that the spiral in the disc persists well after the mode has saturated, and has not fully decayed even by $t = 304$. This simulation employed sectoral harmonics $0 \leq m \leq 8$, and the $m = 2$ seed amplitude was boosted.

instabilities having similar growth rates at both $m = 2$ and $m = 3$, as shown in Figure 6. The growth rate of groove modes is enhanced by the disc supporting response, which is directly related to swing-amplification (see §2.1). In our half-mass Mestel disc model, the swing-amplification parameter $X = 2$ for $m = 2$ and $X = 4/3$ for $m = 3$, and these values straddle the amplification peak (Toomre 1981; Binney & Tremaine 2008) causing the two modes to grow at very similar rates. The red lines in this figure are from a simulation in which we perturbed the quiet start to enhance the seed amplitude at $m = 2$, while the green lines show the consequence of enhancing the $m = 3$ seed amplitude. This trick enables us to study the saturation of each mode separately, while the growing amplitude of the second mode remains sufficiently low that it has a negligible effect on the saturation of the dominant mode. Disturbance forces in both these simulations included multiple sectoral harmonics: $0 \leq m \leq 8$ for the case with $m = 2$ enhanced and $0 \leq m \leq 12$ for the other case. We have confirmed by fitting modes, that the *linear* growth rate, as is

also evident from this Figure, and the pattern speed of each mode is unaffected by the amplitude of the other.

However, the non-linear evolution is mildly changed when multiple sectoral harmonics contribute to the disturbance forces, as illustrated in Figures 7 and 8. The upper left panels of both figures reconfirm that the linear growth of a mode is unaffected by the inclusion of other harmonics, but the saturation amplitude is mildly affected, as is more clearly illustrated by the linear scale in the lower panels. The RH panels reveal that the mode in the LH panels drives a response at twice the angular periodicity, which does not begin at first, but kicks in after a little while. This driven response has identically the same pattern speed as the main mode and rises exponentially at a steeper rate to saturate at about the same time as the driving mode. This behaviour is almost identical in both the green and red lines, even though the red curve is from a simulation in which many sectoral harmonics contributed to the disturbance forces and the green curves just two. In fact, apart from the linear instability whose seed amplitude was depressed (Figure 6), we could find no evidence

Table 2. Mode frequencies (with $N = 6$ million)

m	Q	w_L	$\omega = m\Omega_p + i\beta$
2	1.5	0.2	$0.282 \pm 0.000 + (0.046 \pm 0.001)i$
2	1.8	0.2	$0.283 \pm 0.000 + (0.033 \pm 0.001)i$
2	1.2	0.2	$0.282 \pm 0.001 + (0.064 \pm 0.001)i$
2	1.5	0.3	$0.283 \pm 0.001 + (0.049 \pm 0.001)i$
2	1.5	0.1	$0.283 \pm 0.000 + (0.039 \pm 0.000)i$
2	1.5	0.05	$0.285 \pm 0.000 + (0.029 \pm 0.000)i$
3	1.5	0.2	$0.447 \pm 0.001 + (0.047 \pm 0.001)i$

for strongly growing signal at any m other than that shown in each of these Figures.

The lower LH panels indicate a mild variation in the saturation amplitude of the dominant mode, which is likely caused by the driven responses illustrated on the right. We have not found any evidence that the peak amplitude varies systematically with the addition of extra forcing terms in the six models shown in these two figures. We therefore suspect that the differences are due to the relative phases of the dominant mode and of the driven response. Note that the $m = 6$ driven response peaks at a significantly lower amplitude (Fig. 8) than the corresponding $m = 4$ response (Fig. 7), and that the saturation amplitude spread of the dominant mode is much less.

If this hypothesis is correct, it adds a degree of randomness to the saturation amplitude, although the spread remains small.

3.8 Complete evolution

Figure 9, taken from the case with multiple active sectoral harmonics ($0 \leq m \leq 8$) and the seed amplitude of $m = 2$ slightly boosted, reveals that the spiral disturbance persists for some time after the linear mode has saturated. The second $m = 2$ instability, caused by ILR scattering of the first mode, may be seen in the inner parts. This behaviour is barely distinguishable from that in an $m = 2$ only simulation, and it seems that inclusion of additional harmonics has at most a very minor effect on the overall evolution.

4 OTHER MODELS

We have experimented with changing the properties of the disc, of the groove, and changing the active sectoral harmonic. Note that all the experiments reported in this section employ disturbance forces that are restricted to a single sectoral harmonic: mostly $m = 2$, but $m = 3$ in one case. The measured saturation amplitude therefore avoids the random element caused by the influence of the driven response (§3.7). Also there is no need to enhance the seed amplitude, and we employ the standard quiet start (Sellwood 1983).

The fitted eigenfrequencies of the linear mode in each case are given in Table 2. Notice that the fitted frequency in the first case listed in the table, for which $N = 6$ million particles, is in near perfect agreement with that when $N = 60$ million (§3.1) and when $N = 0.6$ million (Sellwood & Binney 2002).

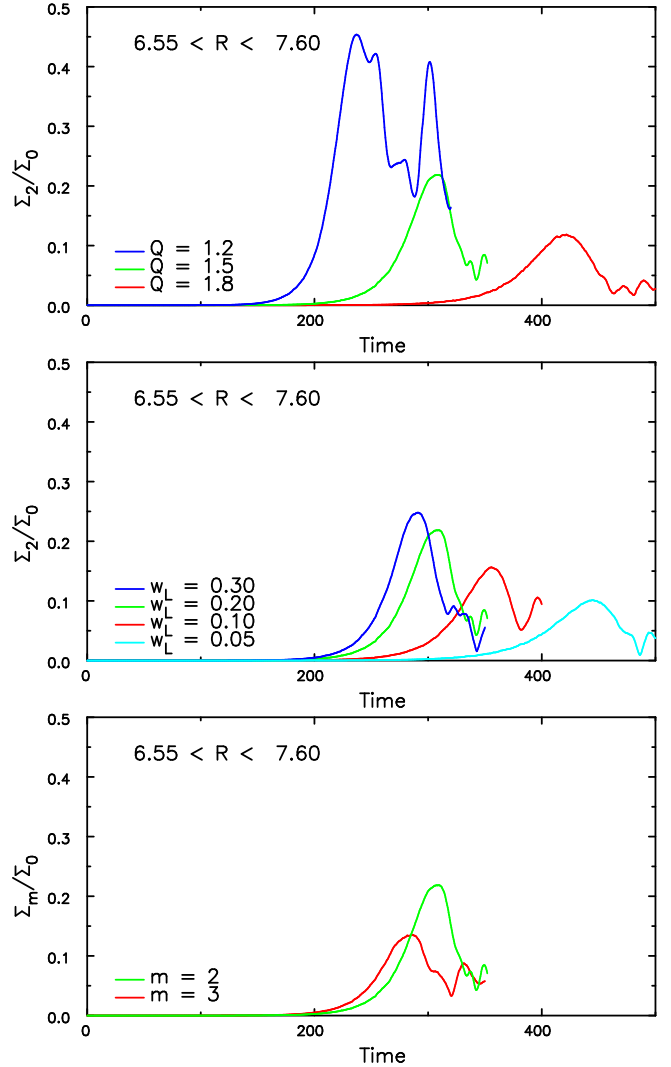


Figure 10. The time evolution of the relative perturbed surface density, averaged over the given radial range, in a series of models. In the top panel, the Q value for the Mestel disc is varied while the groove parameters are held constant, in the middle panel, the width of the groove is changed while Q is held constant, and in the bottom panel, the sectoral harmonic is varied, while the groove parameters and Q are held constant. The green curve in all three panels is from the same simulation.

4.1 New findings

Figure 10 reports the time evolution of the mean relative amplitude of the disturbance density around the radius of corotation. The top panel shows the effect of changing the nominal value of Q of the Mestel disc, while keeping the groove parameters unchanged. It is clear that both the growth-rate and saturation amplitude of the groove mode decrease with increasing Q ; the pattern speed, which is strongly tied to the circular angular frequency at the radius of the groove, remains nearly the same, however (Table 2). The growth rate is enhanced by the supporting response from the disc surrounding the groove, as described in §2.1, which becomes more vigorous with decreasing Q .

The middle panel of Figure 10 shows the effect of varying the groove width, while holding $Q = 1.5$. As expected

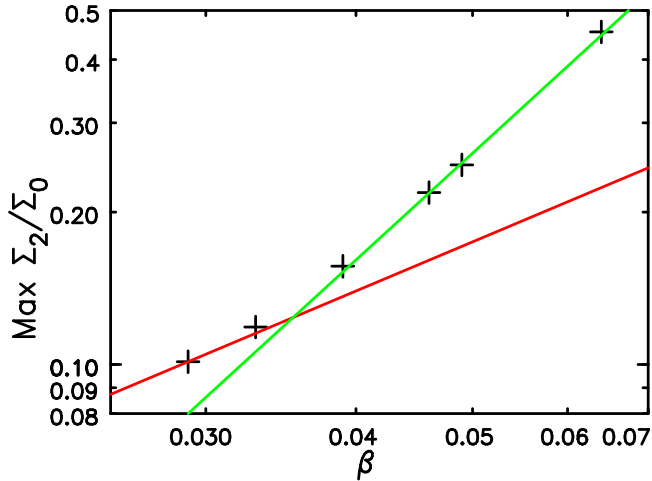


Figure 11. The growth rate dependence of the saturation amplitude of the $m = 2$ modes shown in the top two panels of Figure 10. The points do not fit a straight line even with logarithmic scaling. The red and green lines, which have slopes 1 and 2, respectively are not fits to the points and are drawn only to guide the eye.

from theory for narrow grooves (Sellwood & Kahn 1991), the growth rate of the mode increases with the width of the groove. Once again we see that the saturation amplitude varies with the growth rate of the mode.

The bottom panel of Figure 10 shows the effect of changing the active sectoral harmonic from $m = 2$, which is the default for all other simulations, to $m = 3$.

4.2 Dependence on growth rate

The top two panels of Figure 10 indicate that the saturation amplitude of the mode is lower for more slowly growing modes. In fact, Figure 11 reveals quite a tight correlation for these six cases. Note that our measured growth rates, β , have small uncertainties, but we have no information about possible uncertainties in the limiting amplitude, which would have required us, for example, to have run ensembles of simulations for each case having different random seeds. Note also that had we included other sectoral harmonics, the amplitude peaks may have been slightly affected in an unpredictable manner, as described in §3.7, making the correlation less tight. However, as we have often found, the simpler physics in these restricted cases enables us to learn more.

The logarithmic scaling in Figure 11 indicates that the functional relation between growth rate and saturation amplitude dependence is not a simple power law, which we have been unable to explain. However, the referee suggested that the saturation amplitude should vary as β^2 , which appears to fit the more vigorous instabilities but is inconsistent with the two most slowly growing modes. The argument was based on the expected libration times of orbits trapped at the CR, which unfortunately would be best defined for the most slowly growing modes.

We offer the following qualitative explanation for the interdependence of growth rate and saturation amplitude in terms of the saturation mechanism proposed above (§3.3). There we argued that growth was halted by orbit deflections that are particularly large near the corotation radius of the mode be-

cause particles drift slowly relative to the perturbation. In fact, it is reasonable that the saturation amplitude should increase as the growth rate increases because the perturbation acts on the orbits for a shorter period. Since changes to the unperturbed orbits depend on *both* the amplitude of the perturbation and the length of time that it acts, disturbances reach higher amplitudes for vigorous instabilities than for those from more slowly growing modes, consistent with our results.

The distortions to the rings of test particles at the times the mode saturates are quite similar in the three cases having different Q (Figure 12), consistent with this being a threshold distortion that is reached at lower amplitude because the perturbing forces act for longer when the mode grows slowly. A more careful examination of the Figure shows that radial displacements are slightly smaller for the more slowly growing mode (RH panel) and greater for the rapidly evolving case (LH panel) and these differences become more pronounced at later times.

The quasi-steady density-waves proposed by Bertin *et al.* (1989), if they occur at all, have a different mode mechanism, and therefore may not saturate in the same manner. However, the tight relation revealed in Figure 11 suggests that the very slowly growing modes they favour may saturate at a tiny amplitude. This would be because large orbit deflections in the vicinity of corotation will inevitably build up over the long growth time, leading to the breakdown of the linear approximation and mode saturation at small amplitude.

The different saturation amplitudes for changes to the sectoral harmonic reported in the bottom panel of Figure 10 cannot, however be attributed to growth rate differences. In fact, the instabilities at $m = 2$ and $m = 3$ grow almost equally fast (Table 2) in the linear regime, for the reason given in §3.7. It seems likely that saturation amplitude differs because the spatial scales of the spiral instabilities differ, and growth is limited by the scale of the orbit perturbations relative to the spatial scale of the mode, as illustrated in Figure 13. This argument suggests that, other things being equal, the saturation amplitude of spiral modes should also decrease as the order of rotational symmetry increases.

5 CONCLUSIONS

We have presented an in-depth study of how a single unstable spiral mode in a simplified model ceases to grow and the manner in which it decays. The end of exponential growth is quite abrupt (Figure 1), and is associated with large changes to the orbit guiding centres in the vicinity of corotation (Figure 2) that destroy the linear density response. These orbit deflections, which do not increase random motion (Figure 5), are also responsible for radial migration (Sellwood & Binney 2002).

The spiral fades gradually after it saturates (Figure 9), persisting for over a full turn while the radial dependence of its amplitude changes (Figure 3) as it travels inward inside corotation, as expected (Toomre 1969). The wave possesses a store of angular momentum that was built up as it grew, but since the net angular momentum of an isolated disc cannot change, the mode has reduced the angular momentum of the inner disc and raised that of the outer (Lynden-Bell & Kalnajs 1972). The negative angular

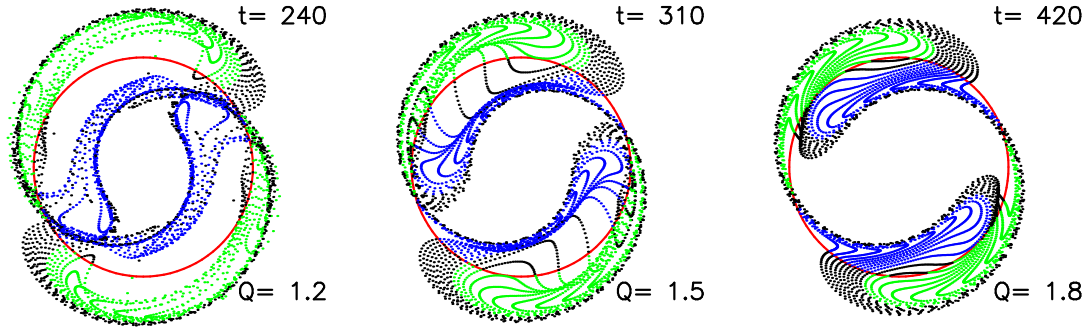


Figure 12. Test particle rings that began in the vicinity of CR only in the three simulations having different Q . The time displayed is when the instability first saturates in each case. Notice that the radial displacements are quite similar in all three cases, even though saturation occurs at very different amplitudes and times.

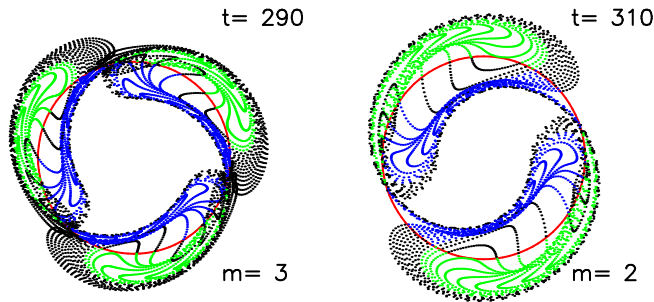


Figure 13. As in Figure 12, but for the two simulations having different m . The time displayed is when the instability first saturates in each case. Notice in the left-hand panel that particle displacements from different spiral arms are beginning to overlap.

momentum stored in the wave drains onto particles at the inner Lindblad resonance, which gain energy and radial action while losing angular momentum. It is noteworthy that we found almost all scattering occurs after the wave has started to decay (Figure 4).

We reported results for other groove modes in §4, finding (Figure 11) a surprisingly tight correlation between the saturation amplitude and the linear growth rate of the mode, in the sense that the maximum amplitude is lower for instabilities that grow more slowly. This is because the more gradual growth of slowly growing modes creates at lower amplitude the large orbit deflections near corotation that destroy the self-consistency requirement of a linear mode. We suggest that this amplitude dependence on growth rate could add a third issue, to the two previously noted in the introduction, why the mechanism for the quasi-steady spiral modes proposed by Bertin *et al.* (1989) seems unlikely to be viable.

The non-linear evolution is only slightly affected by including other sectoral harmonics (Figures 7 and 8). The mild changes to the saturation amplitude would probably blur the correlation in Figure 11 a little, but not change the underlying physical explanation for it.

This series of papers has presented an explanation for the origin and properties of the spirals in simulations of unbarred, isolated, discs that we hope readers will find convincing. Along the way, we have shown that other theories for self-excited spiral patterns in galaxies have multiple issues (§1) and that no other theory accounts for the preference for open, somewhat ragged, spiral patterns having low-order rotational

symmetry that is manifested by real galaxies (*e.g.* Davis *et al.* 2012; Hart *et al.* 2016; Yu *et al.* 2018).

Whether spirals in real galaxies are self-excited by our suggested mechanism is yet to be demonstrated, however, and a meaningful confrontation with observational data is very hard to devise. Observations have established that spiral patterns in real galaxies are azimuthal variations in the surface mass density of the old disc stars (*e.g.* Zibetti *et al.* 2009 and the review by Sellwood & Masters 2022), the gravitational forces from which deflect the gas flow in a systematic manner as it streams through the spiral (*e.g.* Kranz *et al.* 2003; Shetty *et al.* 2007; Erroz-Ferrer *et al.* 2015), conclusively establishing that spirals are density waves in the disc.

As outlined in §1, we argue that spirals may be the superposition of two or more spiral modes that are excited by separate groove instabilities, and it is this statement that is hard to test. Note that evidence will have to be indirect, because we have a single snapshot of each galaxy that is not expected to change significantly for millions of years.

Assuming spiral arms trigger star formation and that stars and gas stream through the pattern, Dixon (1971) and Dobbs & Pringle (2010) proposed that age gradients among the stars downstream from a constant pattern speed arm should become shallower farther from corotation. Foyle *et al.* (2011) rule out age gradients downstream from the spiral in their sample, but others (Chandar *et al.* 2017; Yu & Ho 2018; Miller *et al.* 2019; Peterken *et al.* 2019) claim to have detected them. However, none of these careful studies was able to establish a fixed pattern speed over the entire radial extent of the spiral. Pringle & Dobbs (2019) also suggested that $\cot \alpha$, with α being the pitch angle of the spiral, should have a uniform distribution across some range of α and over spiral arms in many galaxies if spirals wind up over time. Lingard *et al.* (2021) applied this test to a sample of 200 galaxies, finding $\cot \alpha$ values that were consistent with a uniform distribution over the range $15^\circ \lesssim \alpha \lesssim 50^\circ$. However, winding arms are expected (Sellwood & Carlberg 2021) when the spiral results from the superposition of multiple modes having distinct pattern speeds, amplitudes, and perhaps also rotational symmetries.

While the detailed response of gas to spiral arms is an area of current research (*e.g.* Kim *et al.* 2020), we expect its flow to adjust quickly to the slow changes in the spiral potential, and therefore to reflect the instantaneous forcing pattern. But disentangling the projected perturbed velocity flow of

this clumpy medium into its separate contributions from the possible multiple modes, which each have a set of resonances at different radii, presents a considerable challenge, but one which may be possible with observational data of sufficiently high spatial and velocity resolution.

The possible identification of multiple modes would be encouraging, but what really needs to be tested is the mechanism that excites them, which is to show that the distribution of stars in the disc is not a smooth function of their angular momenta. There is little prospect in the foreseeable future to establish the detailed positions and velocity components of a sufficient number stars in any external galaxy that could reveal minor gaps in their phase space distribution. But the *Gaia* satellite is gathering these data for the Milky Way. Sellwood *et al.* (2019) selected from the DR2 (Gaia collaboration 2018) $\gtrsim 300\text{K}$ stars near the Sun having accurate data and small vertical motions, and converted their 4D phase space information into action angle variables, finding a non-smooth distribution in all components but, most tellingly, the kind of scattering features expected from resonant scattering in the distribution of angular momentum, resembling that shown in Figure 4. New data releases will provide more accurate phase space data for more stars, which will be invaluable. But the Milky Way is a strongly barred, mildly warped galaxy having infalling satellites, so that a conclusive finding that features in phase space are due to spiral scattering, and that have excited spiral instabilities, will require very careful modelling. The Milky Way is just one galaxy, and the search for similar confirming evidence from other galaxies is an on-going challenge.

ACKNOWLEDGEMENTS

We thank the referee for insightful comments that have helped us to strengthen our conclusions. JAS acknowledges the continuing hospitality of Steward Observatory.

DATA AVAILABILITY

The data from the simulations reported here can be made available on request. The simulation code can be downloaded from <http://www.physics.rutgers.edu/galaxy>

REFERENCES

- Aumer, M., Binney, J. & Schönrich, R. 2016, MNRAS, **459**, 3326
 Bertin, G. 2014, *Dynamics of Galaxies* 2nd ed. (Cambridge University Press, Cambridge)
 Bertin, G., Lin, C. C., Lowe, S. A. & Thurstans, R. P. 1989, ApJ, **338**, 78-103
 Binney J. & Tremaine S. 2008, *Galactic Dynamics* 2nd ed. (Princeton University Press, Princeton NJ)
 Carlberg, R. G. & Freedman, W. L. 1985, ApJ, **298**, 486
 Chandar, R., Chien, L.-H., Meidt, S., *et al.* 2017, ApJ, **845**, 78
 Davis, B. L., Berrier, J. C., Shields, D. W., *et al.* 2012, ApJS, **199**, 33
 Debattista, V. P. & Sellwood, J. A. 2000, ApJ, **543**, 704
 Dixon, M. E. 1971, ApJ, **164**, 411
 Dobbs, C. & Baba, J. 2014, Publ. Astron. Soc. Australia, **31**, 35
 Dobbs, C. L. & Pringle, J. E. 2010, MNRAS, **409**, 396
 D’Onghia, E., Vogelsberger, M. & Hernquist, L. 2013, ApJ, **766**, 34
 Erroz-Ferrer, S., Knapen, J. H., Leaman, R., *et al.* 2015, MNRAS, **451**, 1004-24
 Foyle, K., Rix, H. -W., Dobbs, C. L., Leroy, A. K. & Walter, F. 2011, ApJ, **735**, 101
 Gaia collaboration: Katz, D., Antoja, T., Romero-Gó, M., *et al.* 2018, A&A, **616A**, 11
 Goldreich, P. & Lynden-Bell, D. 1965, MNRAS, **130**, 125
 Hart, R. E., Bamford, S. P., Willett, K. W., *et al.* 2016, MNRAS, **461**, 3663
 Hockney, R. W. & Brownrigg, D. R. K. 1974, MNRAS, **167**, 351
 Hohl, F. 1971, ApJ, **168**, 343
 Julian, W. H. & Toomre, A. 1966, ApJ, **146**, 810
 Kalnajs, A. J. 1971, ApJ, **166**, 275
 Kim, W.-T., Kim, C.-G. & Ostriker, E. C. 2020, ApJ, **898**, 35
 Kranz, T., Slyz, A. D. & Rix, H.-W. 2003, ApJ, **586**, 143
 Lingard, T., Masters, K. L., Krawczyk, C., *et al.* 2021, MNRAS, **504**, 3364
 Lynden-Bell, D. & Kalnajs, A. J. 1972, MNRAS, **157**, 1
 Miller, R., Kenefick, D., Kenefick, J., *et al.* 2019, ApJ, **874**, 177
 Miller, R. H., Prendergast, K. H. & Quirk, W. J. 1970, ApJ, **161**, 903
 Oort, J. H. 1962, in *Interstellar Matter in Galaxies*, ed. L. Woltjer (New York: Benjamin), p. 234
 Peterken, T. G., Merrifield, M. R., Aragón-Salamanca, A., *et al.* 2019, Nature Astronomy, **3**, 178
 Pringle, J. E. & Dobbs, C. L. 2019, MNRAS, **490**, 1470
 Sellwood, J. A. 1983, J. Comp. Phys., **50**, 337
 Sellwood, J. A. 1989, in *Dynamics of Astrophysical Discs*, ed. J. A. Sellwood (Cambridge: Cambridge University Press) pp 155
 Sellwood, J. A. 2011, MNRAS, **410**, 1637
 Sellwood, J. A. 2012, ApJ, **751**, 44
 Sellwood, J. A. 2014, arXiv:1406.6606 (on-line manual: <http://www.physics.rutgers.edu/~sellwood/manual.pdf>)
 Sellwood, J. A. 2021, MNRAS, **506**, 3018
 Sellwood, J. A. & Athanassoula, E. 1986, MNRAS, **221**, 195
 Sellwood, J. A. & Binney, J. J. 2002, MNRAS, **336**, 785
 Sellwood, J. A. & Carlberg, R. G. 1984, ApJ, **282**, 61
 Sellwood, J. A. & Carlberg, R. G. 2014, ApJ, **785**, 137
 Sellwood, J. A. & Carlberg, R. G. 2019, MNRAS, **489**, 116
 Sellwood, J. A. & Carlberg, R. G. 2021, MNRAS, **500**, 5043
 Sellwood, J. A. & Kahn, F. D. 1991, MNRAS, **250**, 278
 Sellwood, J. A. & Lin, D. N. C. 1989, MNRAS, **240**, 991
 Sellwood, J. A. & Masters, K. L. 2022, ARA&A, **60**, 73
 Sellwood, J. A., Trick, W. H., Carlberg, R. G., Coronado, J. & Rix, H.-W. 2019, MNRAS, **484**, 3154
 Shetty, R., Vogel, S. N., Ostriker, E. C. & Teuben, P. J. 2007, ApJ, **665**, 1138
 Toomre, A. 1969, ApJ, **158**, 899
 Toomre, A. 1981, In *The Structure and Evolution of Normal Galaxies*, eds. S. M. Fall & D. Lynden-Bell (Cambridge, Cambridge Univ. Press) p. 111
 Toomre, A. 1990, in *Dynamics & Interactions of Galaxies*, ed. R. Wielen (Berlin, Heidelberg: Springer-Verlag) p. 292
 Vogelsberger, M., Marinacci, F., Torrey, P. & Puchwein, E. 2020, Nat. Rev. Phys. **2**, 42
 Yu, S.-Y. & Ho, L. C. 2018, ApJ, **869**, 29
 Yu, S.-Y., Ho, L. C., Barth, A. J. & Li, Z.-Y. 2018, ApJ, **862**, 13
 Zibetti, S., Charlot, S., & Rix, H.-W. 2009, MNRAS, **400**, 1181

This paper has been typeset from a $\text{\TeX}/\text{\LaTeX}$ file prepared by the author.